Journal of Atmospheric and Solar–Terrestrial Physics 156 (2017) 1–14

Contents lists available at ScienceDirect

Journal of Atmospheric and Solar–Terrestrial Physics

journal homepage: www.elsevier.com/locate/jastp

Ionospheric F-region observations over American sector during an intense space weather event using multi-instruments

A.J. de Abreu[a,*], I.M. Martin[a], P.R. Fagundes[b], K. Venkatesh[b], I.S. Batista[c], R. de Jesus[c], M. Rockenback[c], A. Coster[d], M. Gende[e], M.A. Alves[a], M. Wild[f]

[a] Instituto Tecnológico de Aeronáutica (ITA), Divisão de Ciências Fundamentais, São José dos Campos, SP, Brazil
[b] Universidade do Vale do Paraíba (UNIVAP), Laboratório de Física e Astronomia, São José dos Campos, SP, Brazil
[c] Instituto Nacional de Pesquisas Espaciais (INPE), São José dos Campos, SP, Brazil
[d] Haystack Observatory, Massachusetts Institute of Technology (MIT), Westford, MA, USA
[e] Facultad de Ciencias Astronómicas y Geofísicas, Universidad Nacional de La Plata (UNLP), La Plata, Argentina
[f] Science and Technology Facilities Council, Rutherford Appleton Laboratory, United Kingdom

ARTICLE INFO

Keywords:
Ionosphere
Ionospheric irregularities
Space weather
Geomagnetic storm

ABSTRACT

The critical interaction between the magnetosphere and ionosphere during intense geomagnetic storms continues to be important to space weather studies. In this investigation, we present and discuss the ionospheric F-region observations in the equatorial, low- and mid-latitude regions in both hemispheres over American sector during the intense geomagnetic storm on 01–03 June 2013. The geomagnetic storm reached a minimum Dst of −119 nT at 0900 UT on 01 June. For this investigation, we present vertical total electron content (VTEC) and phase fluctuations (in TECU/min) from a chain of 10 GPS stations and the ionospheric parameters foF2 and h′F from a chain of 4 digital ionosonde stations, covering from equatorial to mid-latitudes regions over American sector during the entire storm-time period 31 May–03 June 2013. In addition, the plasma density observed from DMSP satellites is presented. The results obtained show that during the sudden impulse/SSC and throughout the main phase of the storm, a large positive phase was observed in mid-latitudes of the northern hemisphere, which could be due to changes in the thermospheric wind circulation. On the other hand, in the mid-latitudes of the southern hemisphere, no deviations are observed in VTEC and foF2 when compared to the quiet period. During the long recovery phase of the storm on 01–02 June, a north-south asymmetry is observed in the F-region. The study confirms the dominant role of the thermospheric winds on north-south asymmetry in the ionospheric F-region. The ionospheric irregularities are found to be confined in the equatorial region, of the bottomside spread-F type, before and during the geomagnetic storm. It shows that the geomagnetic storm did not affect the generation or suppression of ionospheric irregularities at the stations investigated.

1. Introduction

Studies related to space weather in the Sun-Earth system are of great relevance nowadays. The Sun-Earth interaction drastically affects the magnetosphere-ionosphere-thermosphere system causing a variety of physical phenomena, including geomagnetic storms and ionospheric storms. Kamide (2006) mentions that the main goal of space weather is to trace the path of the Sun's energy towards the Earth's upper atmosphere. Space weather is strongly influenced by the speed and density of the solar wind and the interplanetary magnetic field carried by the solar wind plasma during a solar flare and/or coronal mass ejection (CME). As pointed by Buonsanto (1999), unfavorable space weather conditions have significant and adverse effects on increasingly sophisticated ground- and space-based technological systems which are becoming more and more important in public, industrial and civil management/applications (e.g., errors in Global Positioning System (GPS) and in VLF navigation systems, loss of HF communications, and disruption of UHF satellite links due to scintillations). Several researchers have studied the space weather during geomagnetic storms over many years (Kamide et al., 1998; Huang et al., 2003; Jansen and Pirjola, 2004; Heelis et al., 2009; de Abreu et al., 2010a, 2010b, 2011, 2014a; Sahai et al., 2011, 2012; de Jesus et al., 2012; Mansilla and Zossi, 2013, and references therein).

Geomagnetic storms usually start with a sudden storm commence-

* Corresponding author.
E-mail address: abreu.alessandro@gmail.com (A.J. de Abreu).

http://dx.doi.org/10.1016/j.jastp.2017.02.009
Received 7 June 2016; Received in revised form 29 December 2016; Accepted 20 February 2017
Available online 21 February 2017
1364-6826/

ment (SSC), which indicates the arrival of an interplanetary shock structure (the initial phase). However, SSC is not a necessary condition and geomagnetic storms can occur and develop with a gradual storm commencement (GSC). Following the SSC/GSC, sustained southward interplanetary fields *Bz* occur (the main phase) and then a return to normal conditions (the recovery phase) occurs (Gonzalez et al., 1994). During the main phase, the *Bz* component of the solar wind interconnects with the geomagnetic field lines, leading to a large amount of energy input into the high latitude region. On the other hand, during the recovery phase, the energy input minimizes and the geomagnetic activity decreases (Echer et al., 2008).

The response of the ionospheric F-region to a geomagnetic storm is commonly referred as ionospheric storm, which has been studied for decades at different latitudes and longitudes from observations and theoretical models (Prolss, 1993; Bauske and Prolss, 1998; Vlasov et al., 2003; Batista et al., 2006; Foster and Coster, 2007; Sahai et at, 2007a; Astafyeva et al., 2008; Lu et al., 2008; Zhang et al., 2015; de Jesus et al., 2016, and references therein). However, even now complete understandings of the causes of ionosphere storms are not known and this remains one of main issues addressed by the ionospheric community. Ionospheric storms have been categorized by as positive and negative phases. A positive phase results in increased electron density from the median or quiet time values. Otherwise, a negative phase results in decreased electron density from the median or quiet time values (Danilov and Morozova, 1985; Bauske and Prolss, 1998). The physical processes under space weather perturbations responsible for generating of positive and negative phases will be described in the discussions section. However, it is already well known that the ionospheric F-region response during a geomagnetic storm varies significantly with latitude, season, local time, and also by influence of winds and electric fields.

There are two main categories of storm-time electric fields. The first are those generated by prompt or direct equatorward penetration of magnetospheric electric fields from high latitude region. These occur on fairly short time scales (~ few hours or faster). The second main category are those electric fields produced by disturbance dynamo generated by the change in the global winds circulation due to the Joule heating in the high latitude of atmosphere, which are consequences of particle precipitation (Richmond et al., 2003; Maruyama et al., 2005; Klimenko et al., 2011). This second category of storm-time electric fields is typically observed on time scales of several hours. Both prompt penetration and disturbance dynamo electric fields can produce drastic changes in the equatorial, low-, and mid-latitudes of the ionospheric F-region, such as increase or decrease in the F-region height and neutral composition changes.

One of the most fascinating issues of ionospheric physics are equatorial ionospheric irregularities formed in the post-sunset period by process involving **E**×**B** drift variations and the Rayleigh-Taylor instability, which acts in the F-region bottom-side creating perturbations in the electron density (Sultan, 1996). It is important to mention that the signatures of the ionospheric irregularities may occur with a greater or lesser height/time range. The irregularities that are confined in the equatorial region are called medium-scale irregularities or bottom-side spread-F and when they extend to the low latitudes region, they are called large-scale irregularities or plasma bubbles (de Abreu et al., 2014b, 2014c). Past studies have examined both the generation and suppression of equatorial ionospheric irregularities at the equatorial, low-, and mid-latitude regions during geomagnetic storms (e.g., Mendillo et al., 2002; Whalen, 2002; Martinis et al., 2005). Understanding how geomagnetic storms affect the generation/suppression of equatorial irregularities is an issue that requires more investigation as there are significant space weather implications relating to wave propagation in radio communications.

Several works during intense space weather events in northern and southern hemispheres have been reported by Rajaram and Rastogi (1970), Namgaladze et al. (2000), Karpachev et al. (2007), Mendillo and Narvaez (2010), de Abreu et al. (2010b), Balan et al. (2013), de Jesus et al. (2013), and references therein. Rajaram and Rastogi (1970) studied the ionospheric storms using foF2 parameter at pairs of northern and southern mid-latitude stations in different longitude zones, individually for each season, which has shown asymmetry in their behavior, most significantly in the Pacific zone, to some extent in the Asian and American zones. de Abreu et al. (2010b) investigated the ionospheric F-region response in the American sector induced by the intense geomagnetic storm of September 2002 using GPS and ionosonde stations. During the recovery phase of this storm, they observed a strong hemispheric asymmetry and the passage of one traveling ionospheric disturbance (TID) type soliton, inferred for the first time using the data from a chain of ionosondes. Using SUPIM and FORMOSAT-3/COSMIC electron density data measured at the long deep solar minimum (2008–2010), Balan et al. (2013) investigated the longitude variations of the north-south asymmetry of the ionosphere at low latitudes (± 30° magnetic). They reported that, the data and model qualitatively agree and indicate that depending on the longitudes sector both the displacement of the equators and declination angle are important in producing the north-south asymmetry.

Therefore, in this investigation we present and discuss the ionospheric F-region observations at equatorial, low-, and mid-latitude regions in both hemispheres over American sector during an intense space weather event of June 2013 using multi-instrument measurements. For this investigation, we deduced VTEC from GPS stations, plasma density from DMSP satellite, and h′F and foF2 from ionosondes stations. To the authors' knowledge, this is the first time that multi-instruments from ionospheric data are used over American sector to investigate the ionospheric response with respect to the intense geomagnetic storm of June 2013. This case study will expand our understanding of space weather events.

2. Observations

The Global Positioning System (GPS) data were obtained in the standard format known as Receiver Independent Exchange (RINEX) for the 10 stations. The GPS observations were used to obtain the vertical total electron content (VTEC), that is calculated in units of TEC (1 TECU=10^{16} electrons/m^2) (Wanninger, 1993; Brunini et al., 2008) and the rate of change of TEC (phase fluctuations) is calculated in terms of TECU/min (Aarons et al., 1996). The Belém (BELE), Palmas (PAL), Brasília (BRAZ), Presidente Prudente (PPTE), Rio de Janeiro (RIOD), and Porto Alegre (POAL) stations belong to the "Rede Brasileira de Monitoramento Contínuo (RBMC)", operated by the "Instituto Brasileiro de Geografia e Estatística (IBGE)". The Bahia Blanca (VBCA) and Rio Grande (RIO2) stations are operated through the "Serviço de Referência Geocêntrico para as Américas (SIRGAS)". The Greenbelt (GODE) and St. Croix, U. S. Virgin Islands (CRO1) stations belong to the International GNSS Service (IGS) for Geodynamics (Dow et al., 2005). All these stations are located in the American sector from equatorial to mid-latitudes regions in both hemispheres. Fig. 1 and Table 1 provide full details of the GPS sites used in the present study.

The ionospheric sounding stations at Ramey (RMY), Port Stanley (PSTY), USA, and São Luíz (SALU), Fortaleza (FORT), Brazil, are equipped with the Digisonde Portable Sounder (DPS). The RMY and PSTY stations data were obtained from the Digital Ionogram DataBase (DIDBase) by the website http://ulcar.uml.edu/DIDBase/. The SALU and FORT stations data belong to "Instituto Nacional de Pesquisas Espaciais (INPE)". The ionosondes were used to obtain the ionospheric parameters: F-layer minimum virtual height (h′F) and F-layer critical frequency (foF2). Fig. 1 and Table 1 provide full details of the ionosonde sites used in the present study.

The GPS-based TEC maps produced at the NASA Jet Propulsion Laboratory were obtained from http://cdaweb.gsfc.nasa.gov/sp_phys/. The TEC is calculated by mapping GPS observables, carrier-phase and

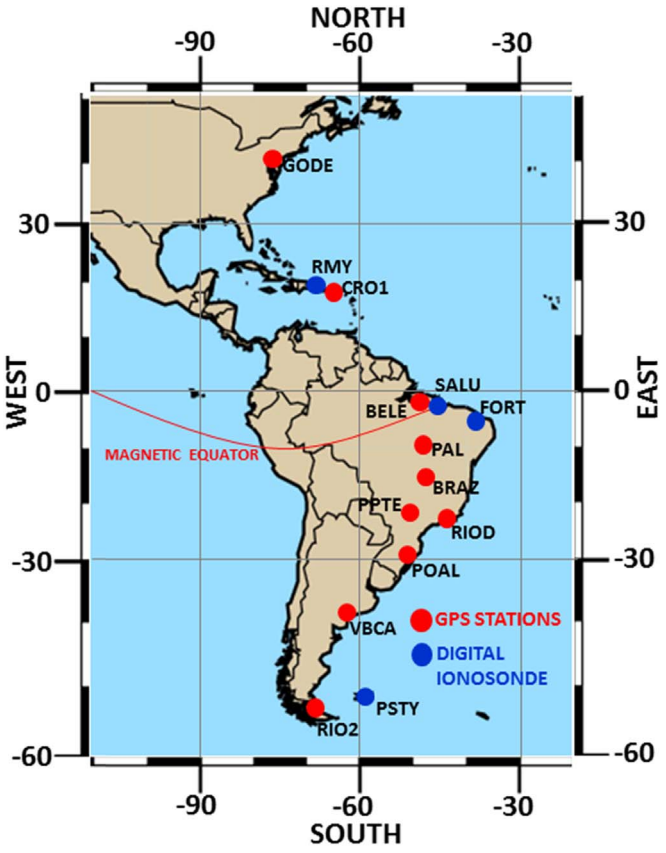

Fig. 1. Map of American sector showing the locations of the GPS stations. The geographical coordinates are shown on the x and y axes. Also, the magnetic equator is shown in red line. (For interpretation of the references to color in this figure legend, the reader is referred to the web version of this article.)

pseudo-range, of dual frequency (L1=1575.42 MHz and L2=1227.60 MHz), collected from IGS ground stations (Dow et al., 2005). The maps produced are used to monitor the space weather. The X-ray flux (1–8 Å) was obtained from GOES satellite by the website http://satdat.ngdc.noaa.gov/sem/goes/data/new_full/. The intensity of geomagnetic indices of the auroral electrojet every 1-min values (AE) and intensity of the ring currents hourly values (Dst) used in the present investigations were obtained from the world data centre (WDC) by the website http://wdc.kugi.kyoto-u.ac.jp. The geomagnetic index indicating storm intensity in 3-hourly values (Kp) were obtained from the website http://ftp.gwdg.de./pub/geophys/kp-ap/tab/. The total interplanetary magnetic field (IMF) of the Bz component (IMF-Bz) in geocentric solar magnetospheric (GSM) coordinates, and solar wind proton bulk velocity

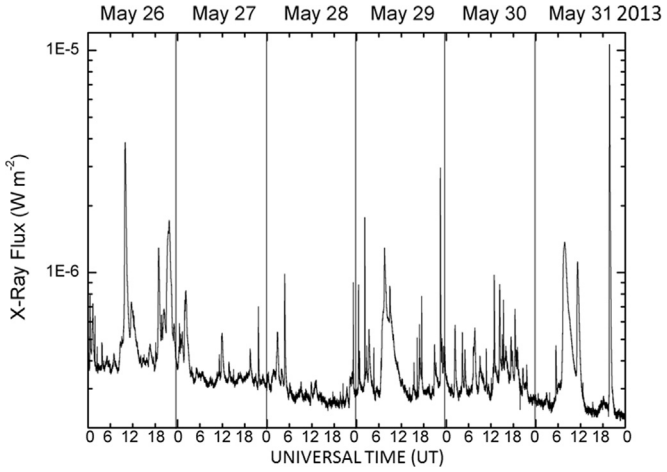

Fig. 2. X-ray flux (1–8 Å) observed from 26 to 31 May 2013 by the GOES satellite.

(Vp), solar wind ion density Np, proton temperature Tp, plasma beta, and dynamic pressure Pdyn were obtained from the Advanced Composition Explorer (ACE) satellite by the website http://www.srl.caltech.edu/ace/. The plasma density measurements on-board the Defense Meteorological Satellite Program (DMSP) F15, F16, F17, and F18 satellites were obtained from the website http://www.ngdc.noaa.gov/stp/satellite/dmsp/.

3. Results and discussion

3.1. Magnetosphere-ionosphere coupling

Fig. 2 shows the time variations of the X-ray flux from GOES satellite for the period of 26–31 May 2013. The X-ray flares are classified in the wavelength range 1–8 Å (0.1–0.8 nm), depending on the power flux level ϕ. The beginning of a C-class solar flare ($10^{-6} \leq \phi \leq 10^{-5}$) is observed in Fig. 2. The day before the start of the storm (31 May), a solar flare with the peak reaching 10^{-5} W m^{-2} is observed around 2000 UT. This X-ray flux is found to be more intense when compared to the previous days 26–30 May. C-class solar flares are considered low intensity, but still can produce coronal mass ejections (CMEs) (Sahai et al., 2007b; Youssef, 2012). Fig. 3 shows the time variations of the total interplanetary magnetic field (IMF-B), IMF of the Bz component (IMF-Bz), solar wind proton velocity (Vp), solar wind ion density (Np), proton temperature (Tp), plasma beta, dynamic pressure (Pdyn), and geomagnetic indices auroral electrojet (AE), storm intensity (Kp), and disturbance storm time (Dst) for the period of 31 May to 03 June 2013. The black vertical arrow and dashed line indicate the sudden storm commencement (SSC). The first sudden

Table 1
Details of the Global Positioning System (GPS) and Digital Ionosonde (DI) sites used in the present study.

Location	Symbol used	Inst.	Lat.	Long.	Dip Lat.	Local time (LT)
Greenbelt	GODE	GPS	39.02° N	76.83° W	48.7° N	LT=UT – 5 h
St. Croix	CRO1	GPS	17.4° N	64.3° W	25.4° N	LT=UT – 4 h
Belém	BELE	GPS	01.4° S	48.4° W	01.8° N	LT=UT – 3 h
Palmas	PAL	GPS	10.2° S	48.2° W	06.1° S	LT=UT – 3 h
Brasília	BRAZ	GPS	15.9° S	47.9° W	11.7° S	LT=UT – 3 h
Presidente Prudente	PPTE	GPS	22.1° S	51.4° W	14.9° S	LT=UT – 3 h
Rio de Janeiro	RIOD	GPS	22.8° S	43.3° W	19.8° S	LT=UT – 3 h
Porto Alegre	POAL	GPS	30.1° S	51.1° W	20.5° S	LT=UT – 3 h
Bahia Blanca	VBCA	GPS	38.7° S	62.3° W	22.4° S	LT=UT – 4 h
Rio Grande	RIO2	GPS	53.8° S	67.8° W	30.6° S	LT=UT – 4 h
Ramey	RMY	DI	18.5° N	67.1° W	25.8° N	LT=UT – 5 h
São Luíz	SALU	DI	2.3° S	44.6° W	02.4° N	LT=UT – 3 h
Fortaleza	FORT	DI	04.0° S	38.0° W	07.7° S	LT=UT – 3 h
Port Stanley	PSTY	DI	51.6° S	57.9° W	29.9° S	LT=UT – 4 h

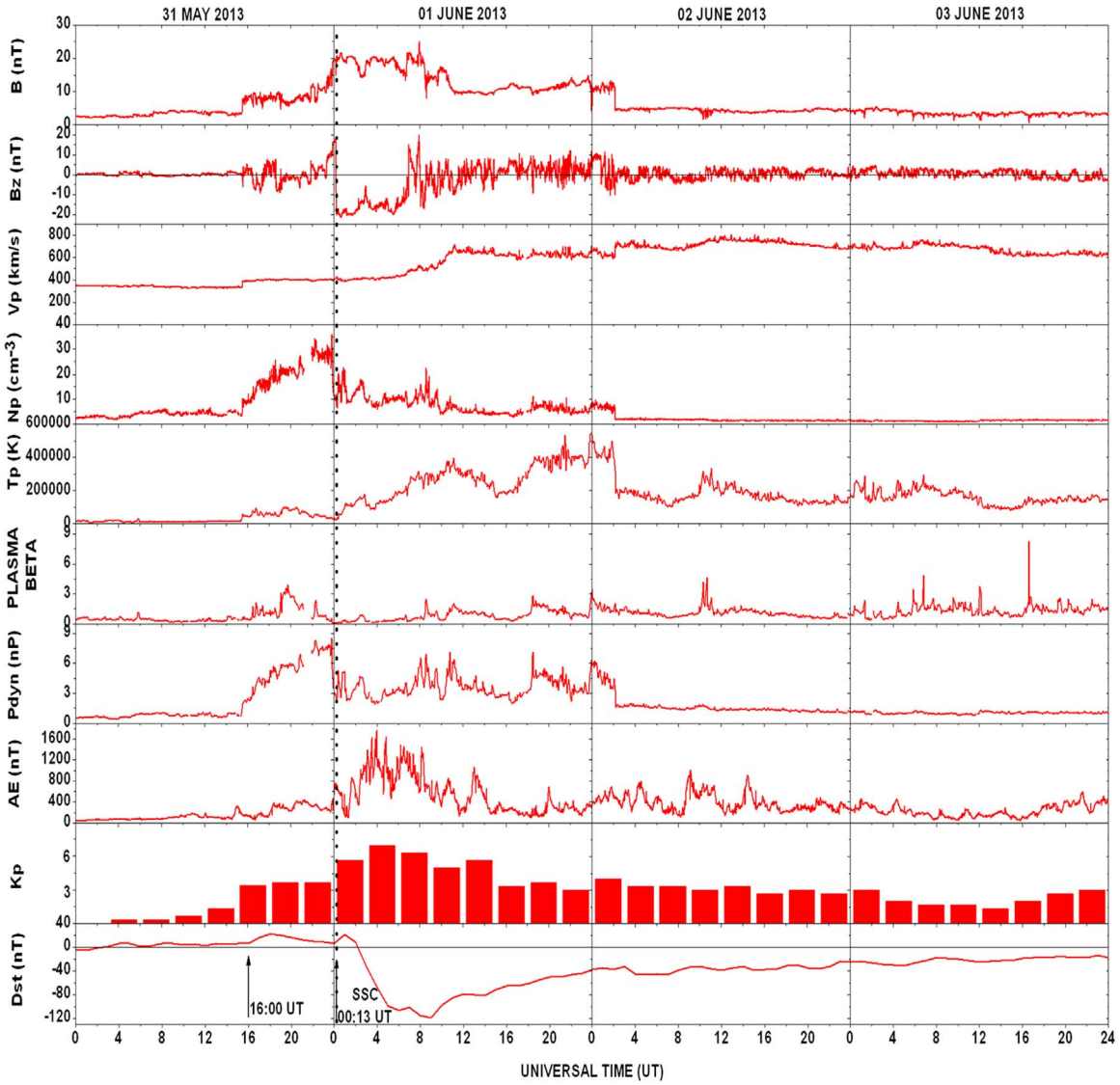

Fig. 3. UT variations of the total interplanetary magnetic field (IMF) B, z component of IMF Bz in GSM coordinates, solar wind proton bulk velocity Vp, solar wind ion density Np, proton temperature Tp, plasma beta, and dynamic pressure Pdyn obtained from the ACE satellite during the period from 31 May to 03 June 2013. Also, The AE, Kp, and Dst geomagnetic indices during the period from 31 May to 03 June 2013 are presented. The black vertical arrow and dashed line indicates the sudden storm commencement (SSC). The arrow shown at 1600 UT indicates the last sudden impulse before the SSC.

impulse occurred at 1600 UT on 31 May and at the same time, all the interplanetary parameters and geomagnetic indices showed large variations from previous hours. The sudden storm commencement (SSC) started at 0013 UT on 01 June. Immediately, the IMF-B reaches about 22 nT and the IMF-Bz turns southward to a value around −20 nT. The Vp remains around 400 km/s during the main phase of the storm and increases to about 700 km/s during the recovery phase, whereas, the Np varies around 20 cm^{-3} after SSC. Also, during the main and recovery phases (days 01–02 June), the Tp, plasma beta, and Pdyn suffered several variations, and therefore, this scenario indicates the arrival of an interplanetary shock structure leading to the formation of an intense geomagnetic storm (see Fig. 3). After the SSC, during the storm main phase, the Kp index reached 7+ at 0500 UT and the Dst index started decreasing from 22 nT at 0100 UT to −119 nT at 0500 UT on 01 June. After 0600 UT on 01 June, the Dst index shows a short recovery of the storm and then decreases again, possibly due to isolated substorm (Wu et al., 2004). After 0900 UT on 01 June to 02 June, the Dst index shows a long storm recovery phase (Fig. 3). Fig. 3 also shows long and strong fluctuations in the AE index from around 0013 UT on 01 June to around 1800 UT on 02 June. During the main and recovery phases, the AE index reached a maximum value of 1800 nT at 0400 UT and of 1000 nT at 1300 UT, respectively. It is an important indicator of large energy injection at auroral latitudes due to the Joule heating (Aksnes et al., 2004).

3.2. Ionospheric response during storm main and recovery phases

Fig. 4 shows the time variations of the vertical total electron content (VTEC) obtained from 10 GPS receiving stations for the period of 31 May to 03 June 2013. The VTEC values for each station were calculated using satellites with elevation angles greater than 20°. The observed VTEC variations during the disturbed period are shown by red lines. The average VTEC variations for quiet periods (five quiet days: 10, 11, 12, 13, and 14 June) are shown with gray bands and their widths correspond to ± 1 standard deviation. The black vertical arrows and dashed lines indicate the sudden impulse and storm commencements (SSC), respectively. The variations of VTEC are observed at the equatorial, low-, and mid-latitudes stations (from GODE to RIO2) over American sector. In the mid-latitude stations in the northern hemisphere (GODE and CRO1), a large positive phase of the storm is

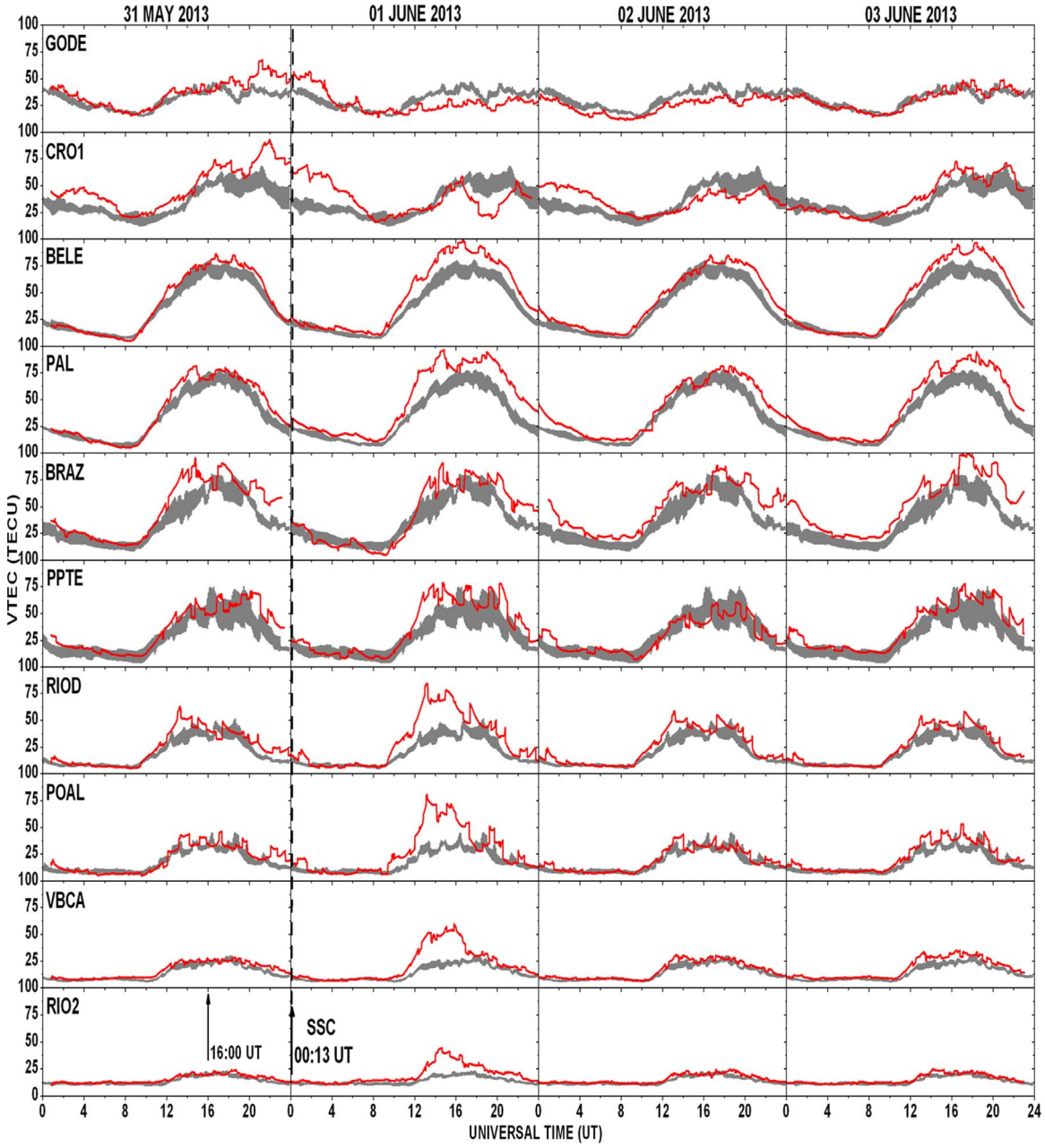

Fig. 4. UT variations of the vertical total electron content (VTEC) from GPS observations obtained from different satellites at 10 GPS stations during the period from 31 May to 03 June 2013 (red lines). The gray bands are ± 1 standard deviation of the average quiet day's values. The black vertical arrow and dashed line indicates the sudden storm commencement (SSC). The arrow shown at 1600 UT indicates the last sudden impulse before the SSC. (For interpretation of the references to color in this figure legend, the reader is referred to the web version of this article.)

seen, possibly due to sudden impulse that occurred at 1600 UT on 31 May and the SSC that occurred at 0013 UT on 01 June. The positive phase remained throughout the main phase of the storm in this region. From the equatorial region to low-latitudes in the southern hemisphere (from BELE to POAL), we observe a weak positive phase compared with the mid-latitude region in the northern hemisphere. In the mid-latitudes in the southern hemisphere (VBCA and RIO2) the VTEC do not show any significant deviations compared to the quite time behavior between 0000 and 0900 UT on 01 June. The global TEC maps at every 2 h are presented in Fig. 5 to investigate the global change in the electron density distribution during the sudden impulse/SSC, main phase, and end of the recovery phase of the intense geomagnetic storms on 31-01-02 June 2013, respectively. The comparative study of a quiet period (before 1600 UT on 31 May) and disturbed periods (after 1600 UT on 31 May) reinforces our observations shown in Fig. 4, focusing mainly on the American sector. The global maps showed in Fig. 5 estimates the TEC (increase or decrease of ionization) at a wide viewing angle. During the main and recovery phases of the storm compared to the previous period (day 31), it is possible to observe a greater ionization on the American sector, corroborating with the TEC observed in Fig. 4. Fig. 6a and b show plasma density measurements on-board the DMSP F15, F16, F17, and F18 satellites during the day time orbiting at an altitude of 840 km every 35 min for the periods from 31 May to 01 June and from 02 to 03 June 2013, respectively. Fig. 6a and b show several of the DMSP F15-F18 orbits, which provide very useful information on particle precipitation into the ionosphere along the orbit (Yuan et al., 2008). It is observed that the orbit is fairly close to the 10 GPS stations on the DMSP F15-F18 plasma-density plots. Each panel is for one satellite pass and the corresponding satellite orbit is shown in the bottom right

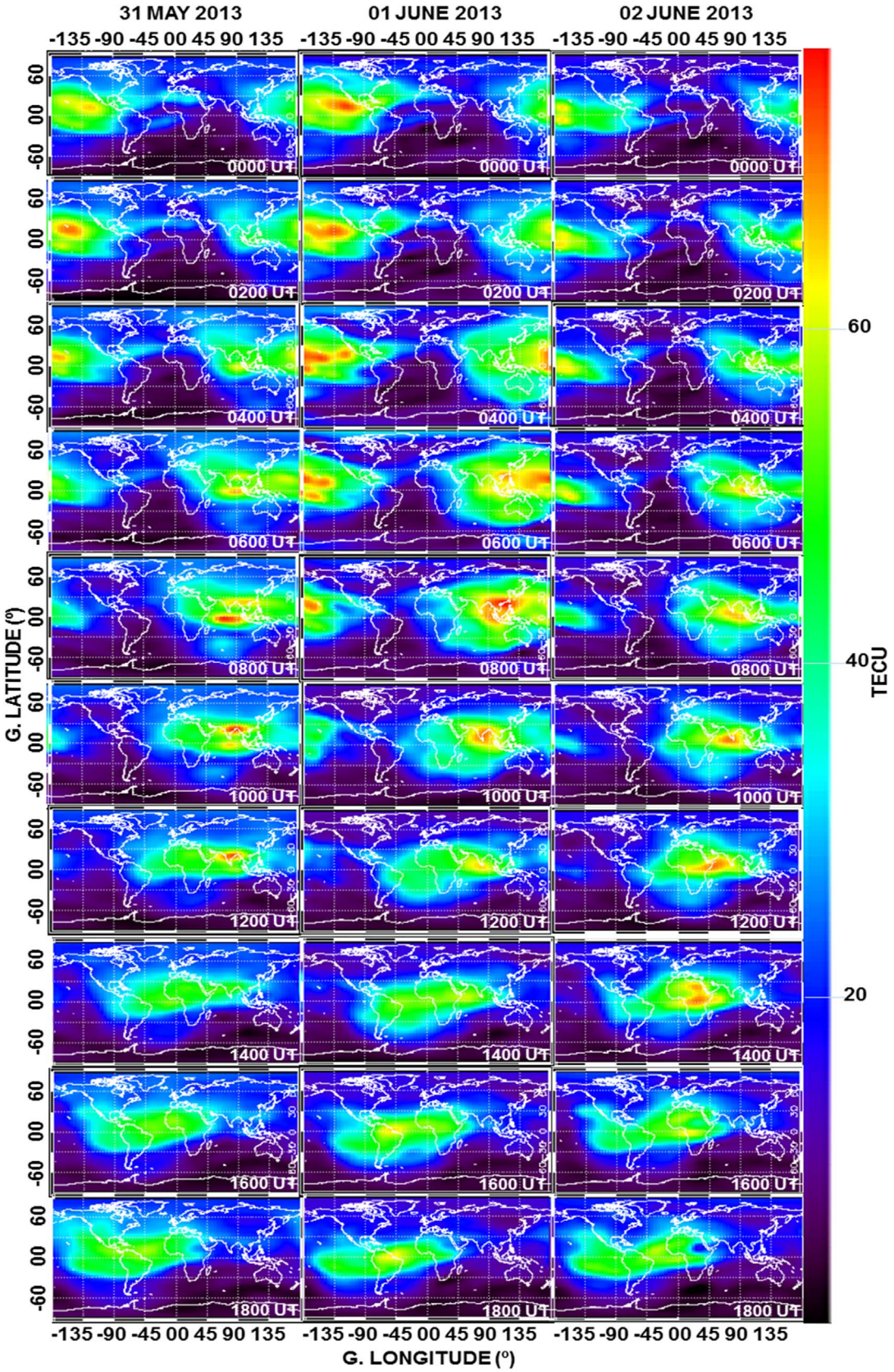

Fig. 5. GPS-TEC maps during the geomagnetic storm from 31 May to 03 June 2013.

panel, for each day. It is important to mention that the plasma density variations increase significantly in northern hemisphere on 31 May after the sudden impulse. During the main phase of the storm on 01 June, the plasma density undergoes strong variations in the northern and southern hemispheres. Unfortunately, the DMSP F15-F18 orbits do not show the plasma density variations at nighttime. However, the

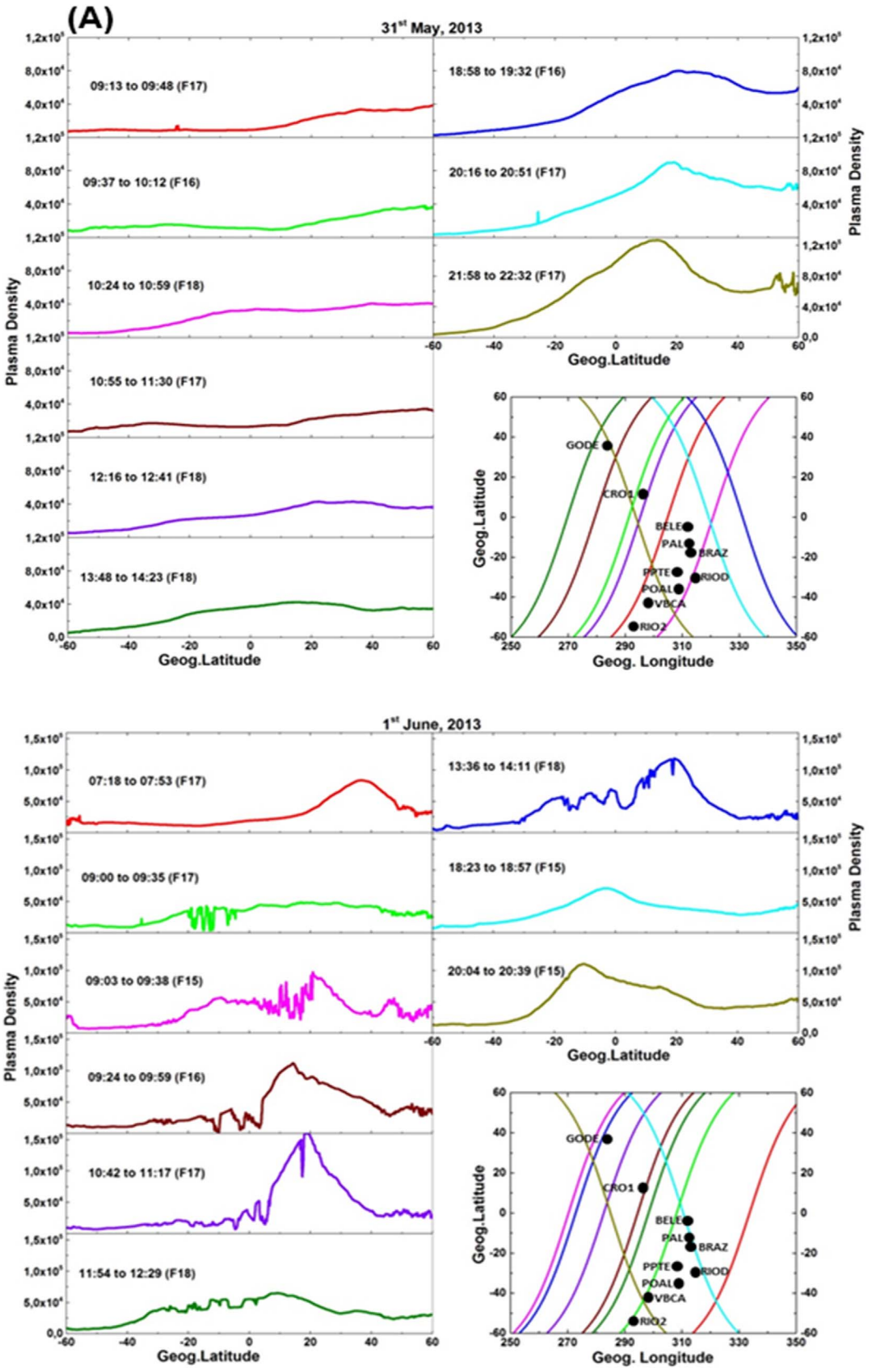

Fig. 6. a UT variations of the plasma density observed from the DMSP F15, F16, F17, and F18 satellites orbiting at an altitude of about 840 km during the intense geomagnetic storm from 31 May to 01 June 2013. **6b –** UT variations of the plasma density observed from the DMSP F15, F16, F17, and F18 satellites orbiting at an altitude of about 840 km during the intense geomagnetic storm from 02 to 03 June 2013.

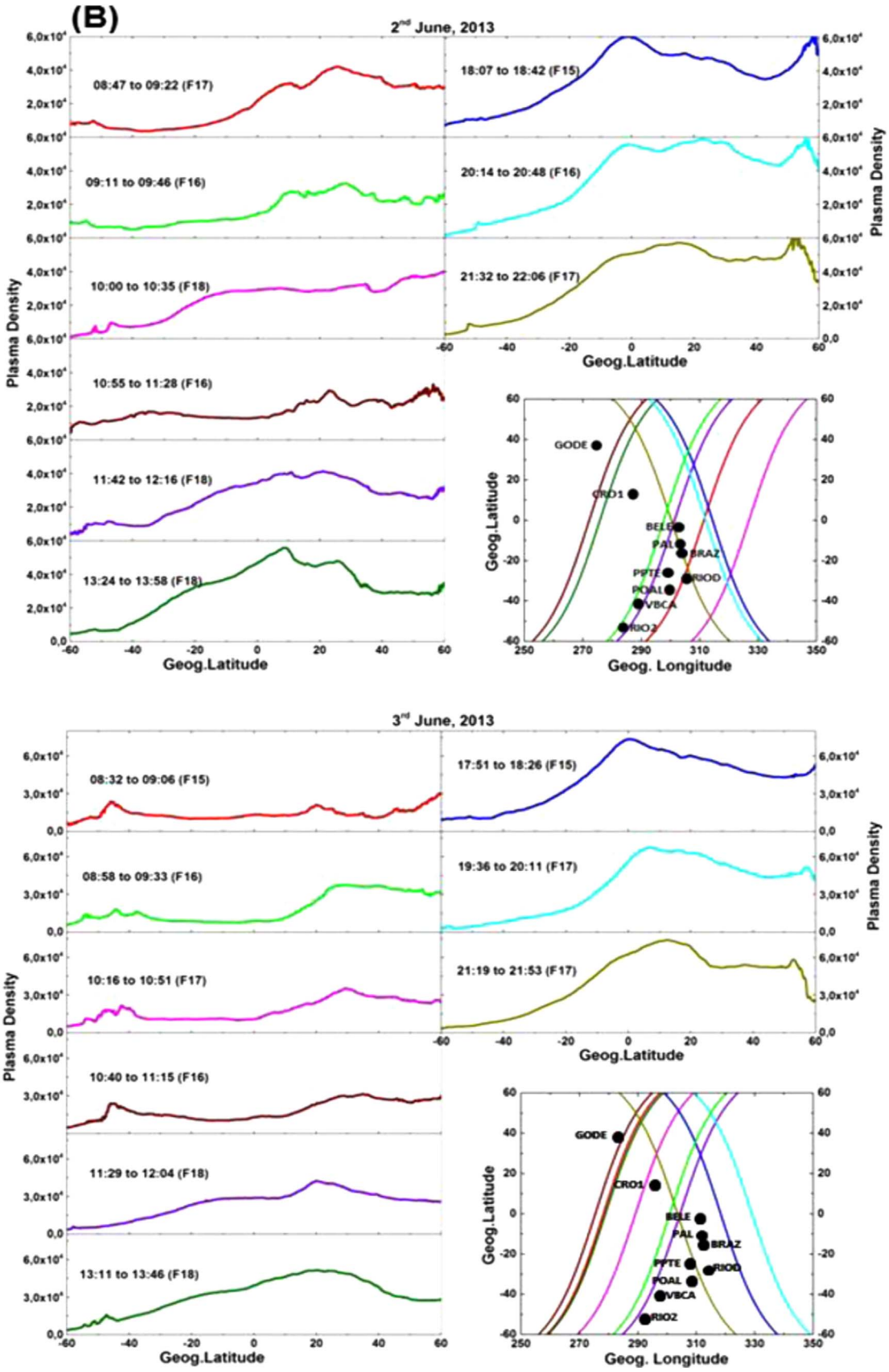

Fig. 6. (*continued*)

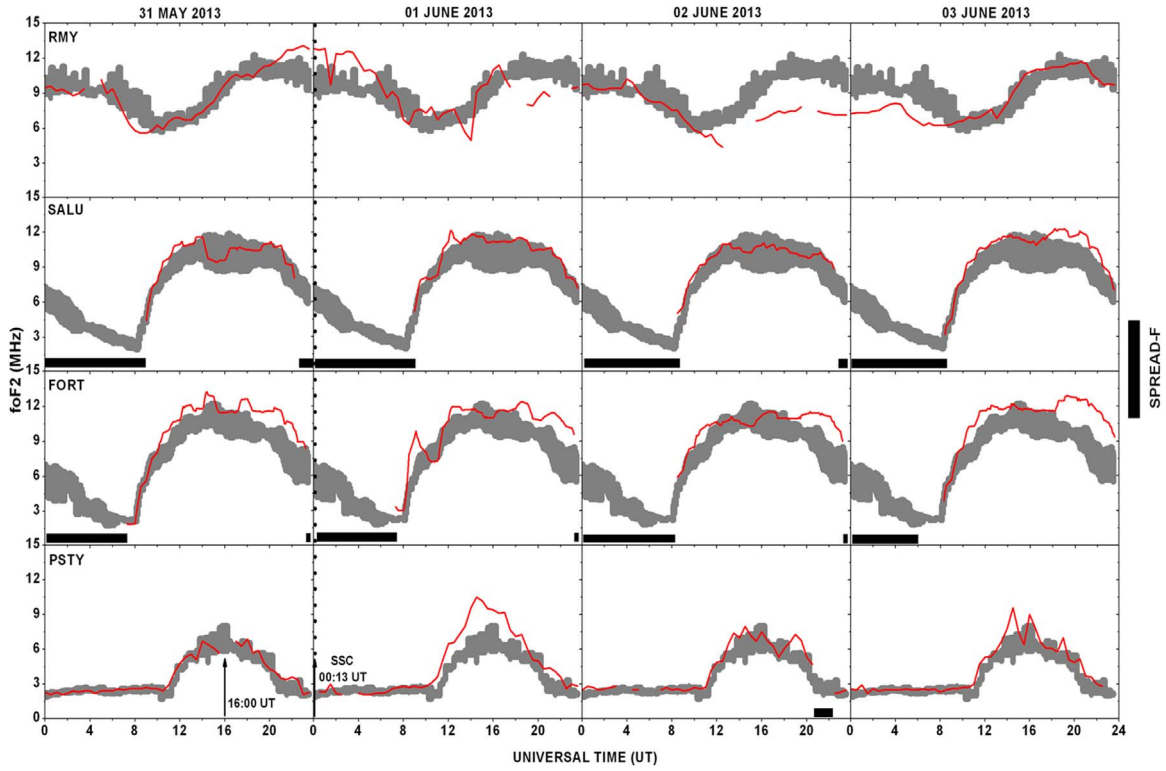

Fig. 7. UT variations of the ionospheric parameter foF2 obtained at Ramey (RMY), São Luís (SALU), Fortaleza (FORT), and Port Stanley (PSTY) stations during the period from 31 May to 03 June 2013 (red lines). The gray bands are ±1 standard deviation of the average quiet day's value. The black vertical arrow and dashed line indicates the sudden storm commencement (SSC). The arrow shown at 1600 UT indicates the last sudden impulse before the SSC. The periods of occurrence of the ESF are indicated with horizontal black bars.

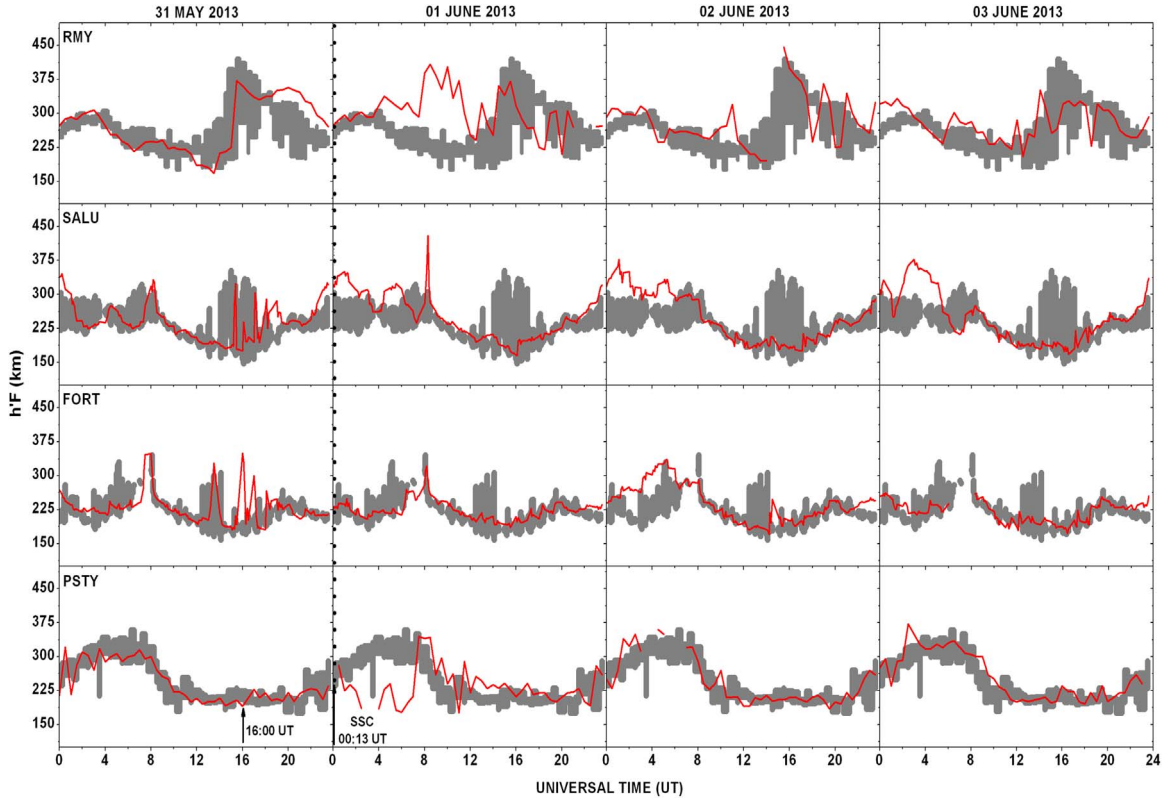

Fig. 8. UT variations of the ionospheric parameter h′F obtained at Ramey (RMY), São Luís (SALU), Fortaleza (FORT), and Port Stanley (PSTY) stations during the period from 31 May to 03 June 2013 (red lines). The gray bands are ±1 standard deviation of the average quiet day's value. The black vertical arrow and dashed line indicates the sudden storm commencement (SSC). The arrow shown at 1600 UT indicates the last sudden impulse before the SSC.

observations follow in agreement with the VTEC at daytime. The time variations of the ionospheric parameters foF2 and h′F obtained from 04 ionosonde stations over American sector for the period of 31 May to 03 June 2013 are shown in Figs. 7 and 8, respectively. The ionospheric parameters foF2 and h′F variations during the disturbed period are shown by red lines. The RMY and PSTY (mid-latitudes regions) and SALU and FORT (equatorial region) were obtained every 30 and 15 min from the ionograms, respectively. The average foF2 and h′F variations (five quiet days: 10, 11, 12, 13, and 14 June) are shown with gray bands and their widths correspond to ± 1 standard deviations. The periods of occurrence of the ESF are indicated with black bars (Fig. 7). The black vertical arrows and dashed line indicate the sudden impulse and sudden storm commencement (SSC), respectively. In mid-latitude in the northern hemisphere (RMY) a positive phase is observed in the foF2 variations during the sudden impulse and the SSC, which also remained during most of the main phase of the storm. In the equatorial region (SALU and FORT), a weak positive phase was observed, while over the mid-latitudes in the southern hemisphere (PSTY), the foF2 variations do not show any deviations. Comparing the VTEC and foF2 parameters, similar results were observed during the SSC and main phase of the storm (Figs. 4 and 7). The h′F at mid-latitude in the northern hemisphere (RMY) shows an increase in the F-region when compared to the quiet period after the sudden impulse. The SALU station in the equatorial region also showed an increase in the F-region, which is observed before and after the occurrence of SSC. The same is not observed at the FORT station, which remained unchanged. However, in the mid-latitudes in the southern hemisphere (PSTY), the h′F is similar to the quiet period during the sudden impulse but it decreases after the SSC. Meanwhile, during the main phase there was a decrease in the F-region height, which possibly did not create conditions for an increase of VTEC and foF2 in this region (see Figs. 4, 7 and 8).

The Dst index shows a long recovery phase, which began around 0900 UT on 01 June until the end of the following day of 02 June (see Fig. 3). At the beginning of the recovery phase an asymmetry is noticed, in which there is a negative phase at mid-latitude in VTEC in the northern hemisphere (GODE and CRO1) and a positive phase at mid-latitude in the southern hemisphere to equatorial region (from RIO2 to BELE). Both positive and negative phases remained until the beginning of 02 June. After this period, there was almost a normalization of VTEC compared to the quiet period in all regions (Figs. 4 and 5). The DMSP satellites show significant variations of plasma density, mainly on 01 June, when the recovery phase was more intense, reaching quiet geomagnetic conditions in the following days (Fig. 6a and b). The same behavior is observed in the diurnal variations of foF2 (Fig. 7), which showed a negative phase at mid-latitude in the northern hemisphere (RMY) and a positive phase from mid-latitude in the southern hemisphere to equatorial region (from PSTY to SALU). During the period of the recovery phase, the h′F has not shown major changes compared to the quiet period. However, in the first hours on 02 June, the stations in all regions showed an increase in the F-region height, possibly this rise extended the positive phase of VTEC (see Figs. 4 and 5).

The possible causes for the positive and negative phases in geomagnetically disturbed periods have been investigated in several studies. Therefore, it can be pointed out that the negative phase observed during the recovery phase of the storm in this investigation is related to a decrease in the O/N_2 density ratio. The main source of ionization in the ionospheric F-region is the atomic oxygen O^+ and the main source of recombination is the molecular nitrogen N_2. Therefore, during geomagnetic storms the electron density in the F-region can increase or decrease. This way, the growth and the reduction of the O/N_2 ratio leads to the positive and negative phases in the ionospheric F-region, respectively (Klimenko et al., 2011). However, the growth of the O/N_2 ratio may involve complex physical mechanisms, such as increase in the oxygen density, equatorward thermospheric wind, the electric field uplifting the plasma, downward protonospheric plasma fluxes, plasma redistribution from low latitudes by electric field disturbances, and traveling ionospheric disturbances (TIDs) (Huang et al., 2005; Goncharenko et al., 2007; de Abreu et al., 2014a). As mentioned by Mansilla and Zossi (2013), there are many points about the details of various processes of positive ionospheric storms that remain unclear.

During the sudden impulse until the period of main phase of the storm, there is a large positive phase in the northern hemisphere. The same was not observed in the other regions. After the occurrence of SSC, a fast decrease of the Dst index was observed, during which there is prompt penetration of magnetospheric electric fields into higher latitude of the ionosphere towards the equatorial region with immediate effects in all latitudes. However, the observations do not show this behavior. On the other hand, during the recovery phase, a negative phase in the northern hemisphere is observed while a positive phase is seen from the mid-latitudes in the southern hemisphere to the equatorial region. In both phases of the storm, the AE index suffered severe changes, reaching 1600 nT during the main phase and 1000 nT during the recovery phase, indicating that higher energy was injected into the high latitude region in the auroral zone. As a result, the global thermospheric wind circulation changes significantly due to increased Joule heating in consequence of enhanced energy injection. Therefore, our results show the role of the equatorward thermospheric winds in the positive phases observed at equatorial, low-, and mid-latitudes regions (Figs. 4 and 7). It should be noted that the distance from CRO1 to BELE stations is 18° of latitude (about 2000 km away) and possibly the winds towards the equatorial region took around 2 h to propagate from mid-latitudes. This possibly indicates that the positive phase observed in the equatorial region during the recovery phase of the storm had strong influence of the large amount of energy injected into the auroral region during the main phase, in which the AE index reached its highest peak, with subsequent equatorward neutral winds propagation. The scenario does not show any kind of wavelike propagation signatures or TIDs. Studies by Balan et al. (2011) support our results. According to their investigations, the neutral mass density N and electron density Ne at 400 km height measured by CHAMP satellite during nine intense geomagnetic storms show that the effects of the storm time equatorward neutral winds produce the positive storms with and without penetration of electric fields (before their chemical effects become dominant) by reducing (or stopping) the downward diffusion of plasma along the field lines and by raising and supporting the ionosphere at high altitudes of reduced chemical loss (see also Balan et al., 2009). Other researchers also supported this idea. For example, Kil et al. (2003) investigated the response to the geomagnetic storm of July 2000 using GPS-TEC maps and measurements of ion density, composition, and drift velocity from DMSP satellite. They show that the storm-induced equatorward neutral winds are the main driver of the positive ionospheric storm.

It is important to mention that, during the recovery phase an asymmetry in the northern and southern hemispheres is noticed in the present observations. The VTEC and foF2 clearly show a negative phase in the northern hemisphere and a positive phase in the southern hemisphere, which quickly expanded to the equator. The north-south asymmetry in the ionospheric F-region during geomagnetic storms has been reported by several investigators (e.g., Sastri et al., 2008; Danilov, 2013; Thomas et al., 2016). However, the dynamic of the north-south hemispheres is a major factor that contributes to the hemispheric asymmetry (Yigit et al., 2015). As already mentioned above, the thermospheric winds circulation changes play an important role in the electron density variations. The thermospheric winds move the plasma up and down along the geomagnetic field lines and transport the plasma from one hemisphere to the other (Liu et al., 2007). There are significant differences in the strength and configuration of the geomagnetic field between the northern and southern hemispheres. As is well known and also pointed by Forster and Haaland (2015), the ionosphere is magnetically connected to the magnetosphere and this

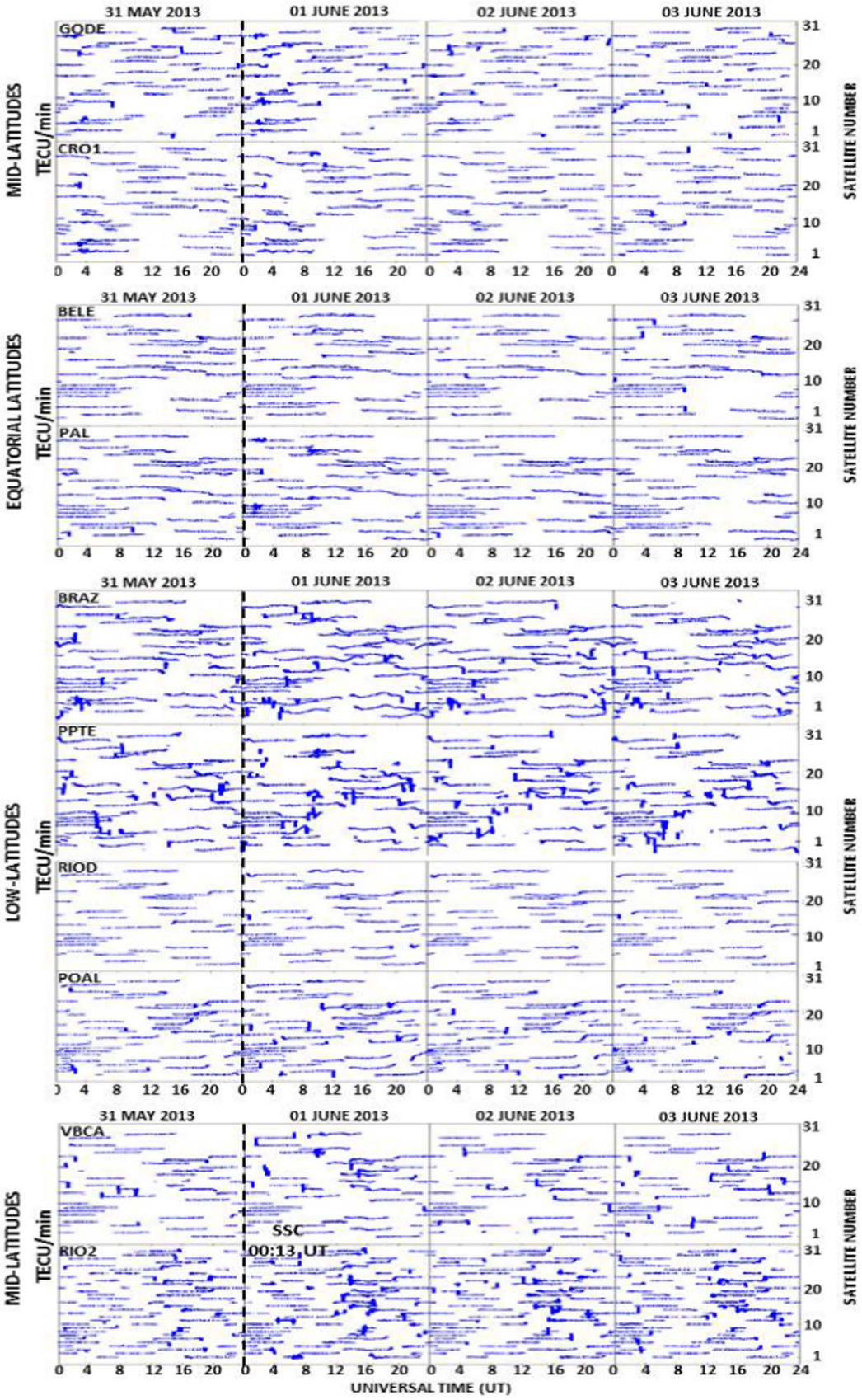

Fig. 9. Rate of change of TEC (phase fluctuations) from GPS observations obtained from different satellites at 10 stations in the American sector during the period from 31 May to 03 June 2013. The black vertical dashed line indicates the sudden storm commencement (SSC).

difference is reflected in the magnetosphere in the form of different feedback from the two hemispheres. Our results support the view of Astafyeva et al. (2004), that during geomagnetic storms, the enhanced Joule heating over high latitudes lifts the neutrals and drives them toward the low and equatorial latitudes, thereby changing thermospheric composition globally. This storm-induced circulation augments the normal seasonal circulation from summer to winter. As a result, in the northern hemisphere, the perturbations can be easily transported to middle and low latitudes than in the southern hemisphere. However, the disturbed ionospheric conditions as a result of thermospheric winds circulation due to increased Joule heating during the intense geomagnetic storm and the geomagnetic field configuration possibly resulted in the strong north-south asymmetry observed in this investigation.

3.3. Equatorial Ionospheric Irregularities

Fig. 7 shows the presence of equatorial spread-F at SALU and FORT stations (equatorial region) for the nights of 30–31 May, 31-01, 01–02, and 02–03 June between about 2200 UT and 0900 UT. Fig. 7 also shows the presence of spread-F at PSTY station (mid-latitude) on 02 June from around 2040 UT to 2230 UT. The spread-F is not observed during any other times on these nights in the low- and mid-latitudes regions in either hemispheres. Fig. 9 shows the rates of change of TEC in TECU/min for individual satellites obtained from 10 GPS stations for the period of 31 May to 03 June 2013. The dashed line indicates sudden storm commencement (SSC). As pointed out by Aarons et al. (1997), the rates of change of TEC may indicate the presence of phase fluctuations, which represent the ionospheric irregularities with size of the order of kilometers (Mendillo et al., 2000; Shagimuratov et al., 2012). In contrast to Fig. 7, in Fig. 9 it is not possible to observe the presence of phase fluctuations in equatorial, low-, and mid-latitudes regions in both hemispheres, characterizing the absence of large-scale irregularities. Ionospheric irregularities detected by the digital ionosonde and GPS stations have different altitudinal ranges and wavelengths. Chen et al. (2006) using digisonde spread-F and GPS phase fluctuations in the equatorial ionosphere showed that the ionospheric irregularities occurring on May, June, July, and August months are less than 3% as compared to the other months of the year. Their observations also showed that the digisonde is more sensitive than the GPS, being able to detect ionospheric irregularities of smaller scales (for more details see Pi et al., 1997). However, studies show that the geomagnetic storms can generate or suppress the occurrence of irregularities (e.g., Martinis, 2005). During disturbances periods, the equatorial electric fields can be affected by prompt penetration of magnetospheric electric field and disturbance dynamo. The equatorial zonal electric field affects the growth rate of the Rayleigh–Taylor instability through of gravitational and electrodynamic drift terms, controlling the electron density gradient in the bottomside of the F-region after sunset (Li et al., 2008). Thus, the generation or suppression can be directly affected. Nevertheless, the observations show that at the stations investigated, the intense geomagnetic storm of 01–03 June did not affect the equatorial electric fields responsible for the generation or suppression of ionospheric irregularities. The irregularities of the spread-F type are observed in the equatorial region on the night before the storm (30–31 May) and in the following nights during the storm (31-01, 01–02, and 02–03 June) (Fig. 7). The spreads-F conditions that are confined in the equatorial region are called bottomside spread-F. Our results are confirmed by Takahashi et al. (2010), where they have used ionosonde stations at SALU and FORT during the storm of 30 September 2005 and reported the bottomside spread-F, which was confined in a narrow height region (~20–50 km) and lasted more than one hour then developing into vertically well extended plasma bubbles. However, the spread-F observed only in PSTY at the end of 02 June must be a phenomena caused by the wave disturbances propagating from mid-latitude indicated by the multiple F-traces in the ionograms, since there was no spread-F closer to the magnetic equator (Pimenta et al., 2008; de Jesus et al., 2012). Therefore, this study shows that there is still an open question in knowing the role of the geomagnetic storms in the generation or suppression of equatorial ionospheric irregularities. Hence, in our future work, we will study the irregularities over American sector for a long period of data with and without occurrences of geomagnetic storms. Thus, we will correlate the storms classified by intensity (low, moderate, intense and, super intense), with the seasonal variations of irregularities in order to amplify the knowledge of the physical mechanisms involved.

4. Conclusions

In this investigation we presented and discussed the ionospheric F-region observations at equatorial, low-, and mid-latitude regions in the northern and southern hemispheres over the American sector during an intense space weather event of June 2013 using GPS stations, DMSP satellites and ionosonde stations. Some of the salient features related to these observations and analysis are summarized below.

We observed that different regions in the American sector responded in different ways to the intense geomagnetic storm of June 2013. From the sudden impulse to the main phase of the storm, only the mid-latitudes in the northern hemisphere were affected. We also observed a large positive phase which could be due to changes in the thermospheric wind circulation.

During the storm recovery phase, from the mid-latitudes in the northern hemisphere to the mid-latitudes in the southern hemisphere were affected. We observed a north-south asymmetry in the ionospheric F-region, with a negative phase at mid-latitudes in the northern hemisphere and a positive phase from mid-latitudes in the southern hemisphere to the equatorial region. Negative phase may be associated with a decrease in the O/N_2 ratio, which the O^+ and N_2 are the main source of ionization and recombination, respectively. On the other hand, the positive phase observed could be due to the changes in the thermospheric wind circulation due to increased Joule heating and the geomagnetic field configuration. The observations did not show any type of wave propagation. Our study confirms the dominant role of the thermospheric winds on north-south asymmetry in the ionospheric F-region.

We observed that the intense storm of 01–03 June at the stations investigated did not influence the generation or suppression of ionospheric irregularities. The observed irregularities presented a seasonal pattern of the bottomside spread-F type.

We concluded from the present observations that the effects of geomagnetic storms on the ionosphere vary appreciably with respect to the phases of the storm and region-to-region. Because the storm time changes in the global dynamics cause significant perturbations in the ionospheric phenomenon and makes it more complex to predict the ionospheric response to the geomagnetic storms. Therefore, it is of significant importance to study the ionospheric response during the geomagnetic storms using observations from various regions through different techniques.

Acknowledgements

Thanks are due to the Brazilian funding agencies for the partial financial support through Grants 402685/2015-6 (CNPq) and 088861/2013 (PVS-CAPES-ITA). The authors thank the authorities of the "Rede Brasileira de Monitoramento Contínuo de GPS (RBMC)", Brazil; "Serviço de Referência Geocêntrico para as Américas (SIRGAS)", Argentina; and International Global Navigation Satellite System (GNSS) Service (IGS) for easy access to their data. The authors thank Dr. Bodo Reinisch for the RMY data obtained from the Digital Ionogram DataBase (DIDBase).

References

Aarons, J., Mendillo, M., Yantosca, R., 1996. GPS phase fluctuations in the equatorial region during the MISETA 1994 campaign. J. Geophys. Res. 101 (A8), 26851–26862.

Aarons, J., Mendillo, M., Yantosca, R., 1997. GPS phase fluctuations in the equatorial region during sunspot minimum. Radio Sci. 32, 1535–1550.

de Abreu, A.J., Fagundes, P.R., Gende, M., Bolaji, O.S., Brunini, C., 2014a. Investigation of ionospheric response to two moderate geomagnetic storms using GPS-TEC measurements in the South American and African sectors during the ascending phase of solar cycle 24. Adv. Space Res. v. 53, 1313–1328.

de Abreu, A.J., Sahai, Y., Fagundes, P.R., de Jesus, R., Bittencourt, J.A., Pillat, V.G., 2011. An investigation of ionospheric F region response in the Brazilian sector to the super geomagnetic storm of may 2005. Adv. Space Res. 48, 1211–1220.

de Abreu, A.J., Sahai, Y., Fagundes, P.R., Becker-Guedes, F., de Jesus, R., Guarnieri, F.L., Pillat, V.G., 2010a. Response of the ionospheric F-region in the Brazilian sector during the super geomagnetic storm in April 2000 observed by GPS. Adv. Space Res. v. 45, 1322–1329. http://dx.doi.org/10.1016/j.asr.2010.02.003.

de Abreu, A.J., Fagundes, P.R., Bolzan, M.J.A., Bolzan, M.J.A., de Jesus, R., Pillat, V.G., Abalde, J.R., Lima, W.L.C., 2014b. The role of the traveling planetary wave ionospheric disturbances on the equatorial F region post-sunset height rise during the last extreme low solar activity and comparison with high solar activity. J. Atmos. Sol. Terr. Phys. V 113, 47–57.

de Abreu, A.J., Fagundes, P.R., Bolzan, M.J.A., Gende, M., Brunini, C., de Jesus, R., Pillat, V.G., Abalde, J.R., Lima, W.L.C., 2014c. Traveling planetary wave ionospheric disturbances and their role in the generation of equatorial spread-F and GPS phase fluctuations during the last extreme low solar activity and comparison with high solar activity. J. Atmos. Sol. Terr. Phys. V 117, 7–19.

de Abreu, A.J., Fagundes, P.R., Sahai, Y., de Jesus, R., Bittencourt, J.A., Brunini, C., Gende, M., Pillat, V.G., Lima, W.L.C., Abalde, J.R., Pimenta, A.A., 2010b. Hemispheric asymmetries in the ionospheric response observed in the American sector during an intense geomagnetic storm. J. Geophys. Res. 115, A12312. http://dx.doi.org/10.1029/2010JA015661.

Aksnes, A., Stadsnes, J., Lu, G., Østgaard, N., Vondrak, R.R., Detrick, D.L., Rosenberg, T.J., Germany, G.A., Schulz, M., 2004. Effectsof energetic electrons on the electrodynamics in the ionosphere. Ann. Geophys. 22, 475–496.

Astafyeva, E.I., Zakharenkova, I., Doornbos, E., 2004. Opposite hemispheric asymmetries during the ionospheric storm of 29-31 August 2004. J. Geophys. Res. 120.

Astafyeva, E.I., Afraimovich, E.L., Voeykov, S.V., 2008. Generation of secondary waves due to intensive large-scale AGW traveling. Adv. Space Res. 41 (9), 1459–1462.

Balan, N., Alleyne, H., Otsuka, Y., Vijaya Lekshmi, D., Fejer, B.G., McCrea, I., 2009. Relative effect of electric field and neutral wind on positive ionospheric storms. Earth Planets Space 61, 439–445.

Balan, N., Yamamoto, M., Liu, J.Y., Otsuka, Y., Liu, H., Luhr, H., 2011. J. Gephys. Res. 116, A07305.

Balan, N., Rajesh, P.K., Sripathi, S., Tulasiram, S., Liu, J.Y., Bailey, G.J., 2013. Modeling and observations of the north-south ionospheric asymmetry at low latitudes at long deep solar minimum. Adv. Space Res. 52, 375–382.

Batista, I.S., Abdu, M.A., Souza, J.R., Bertoni, F., Matsuoka, M.T., Camargo, P.O., Bailey, G.J., 2006. Unusual early morning development of the equatorial anomaly in the Brazilian sector during the Halloween magnetic storm. J. Geophys. Res. 111, A05307 .

Bauske, R., Prolss, G.W., 1998. Numerical simulation of long-duration positive ionospheric storm effects. Adv. Space Res. 22 (1), 117–121.

Brunini, C., Meza, A., Gende, M., Azpilicueta, F., 2008. South American regional ionospheric maps computed by GESA: a pilot service in the framework of SIRGAS. Adv. Space Res. 42, 737–744.

Buonsanto, M.J., 1999. Ionospheric storms – a review. Space Sci. Rev. V 88, 563–601.

Chen, W.S., Lee, C.C., Liu, J.Y., Chu, F.D., Reinisch, B.W., 2006. Digisonde spread-F and GPS phase fluctuations in the equatorial ionosphere during solar maximum. J. Geophys. Res. 111, A12305.

Danilov, A.D., 2013. Ionospheric F-region response to geomagnetic disturbances. Adv. Sp. Res. 52 (3), 343–366.

Danilov, A.D., Morozova, L.D., 1985. Ionospheric storms in the F2 region: morphology and physics (review). Geomagn. Aeron. 25, 593–605.

Dow, J.M., Neilan, R.E., Gendt, G., 2005. The International GPS service (IGS): Celebrating the 10th anniversary and looking to the next decade. Adv. Space Res. 36 (3), 320–326.

Echer, E., Gonzalez, W.D., Tsurutani, B.T., Gonzalez, A.L.C., 2008. Interplanetary conditions causing intense geomagnetic storms (Dst < =100 nT) during solar cycle 23 (1996–2006). J. Geophys. Res. 133, A05221.

Forster, M., Haaland, S., 2015. Interhemispheric differences in ionospheric convection: Cluster EDI observations revisited. J. Geophys. Res. 120.

Foster, J.C., Coster, A.J., 2007. Conjugate localized enhancement of total electron content at low latitudes in the American sector. J. Atmos. Sol. Terr. Phys. 69, 1241–1252.

Goncharenko, L.P., Foster, J.C., Coster, A.J., Huang, C., Aponte, N., Paxton, L.J., 2007. Observations of a positive storm phase on September 10, 2005. J. Atmos. Sol. Terr. Phys. 69, 1253–1272.

Gonzalez, W.D., Joselyn, J.A., Kamide, Y., Kroehl, H.W., Rostoker, G., Tsurutani, B.T., Vasyliunas, V.M., 1994. What is a magnetic storm. J. Geophys. Res. 99 (A4), 5771–5792.

Heelis, R.A., Sojka, J.J., David, M., Schunk, R.W., 2009. Storm time density enhancements in the middle-latitude dayside ionosphere. J. Geophys. Res. 114, A03315.

Huang, C.-S., Foster, J.C., Goncharenko, L.P., Sofko, G.J., Borovsky, J.E., Rich, F.J., 2003. Midlatitude ionospheric disturbances during magnetic storms and substorms. J. Geophys. Res. 108 (A6), 1244.

Huang, C.-S., Foster, J.C., Goncharenko, L.P., Erickson, P.J., Rideout, W., Coster, A.J., 2005. Strong positive phase of ionospheric storms observed by the Millstone Hill incoherent scatter radar and global GPS network. J. Geophys. Res. 110 (A6), A06303 .

Jansen, F., Pirjola, R. Space weather research elucidates risks to technological infrastructure, EOS, Transactions. American Geophysical Union, 85, 2004, pp. 241–245.

de Jesus, R., Fagundes, P.R., Coster, A., Bolaji, O.S., Sobral, J.H.A., Batista, I.S., de Abreu, A.J., Venkatesh, K., Gende, M., Abalde, J.R., Sumod, S.G., 2016. Effects of the intense geomagnetic storm of September-October 2012 on the equatorial, low- and mid-latitude F region in the American and African sector during the unusual 24th solar cycle. J. Atmos. Sol. Terr. Phy. 138-139, 93–105.

de Jesus, R., Sahai, Y., Fagundes, P.R., de Abreu, A.J., Brunini, C., Gende, M., Bittencourt, J.A., Abalde, J.R., Pillat, V.G., 2013. Response of equatorial, low- and mid-latitude F-region in the American sector during the intense geomagnetic storm on 24–25 October 2011. Adv. Space Res. 52, 147–157.

de Jesus, R., Sahai, Y., Guarnieri, F.L., Fagundes, P.R., de Abreu, A.J., Bittencourt, J.A., Nagatsuma, T., Huang, C.-S., Lan, H.T., Pillat, V.G., 2012. Ionospheric response of equatorial and low latitude F-region during the intense geomagnetic storm on 24–25 August 2005. Adv. Space Res. 49, 518–529.

Kamide, Y., 2006. What is an intense geomagnetic storm? Space Weather Q. 4, S06008.

Kamide, Y., Baumjohann, W., Daglis, I.A., Gonzalez, W.D., Grande, M., Joselyn, J.A., Mcpherron, R.L., Phillips, J.L., Reeves, E.G.D., Rostoker, G., Sharma, A.S., Singer, H.J., Tsurutani, B.T., Vasyliunas, V.M., 1998. Current understanding of magnetic storms: storm–substorm relationships. J. Geophys. Res. 103 (A8), 17705–17728.

Karpachev, A.T., Biktash, L.Z., Maruyama, T., 2007. The high-latitude ionosphere structure on 22 March, 1979 magnetic storm from multi - satellite and ground-based observation. Adv. Space Res. 40, 1852–1857.

Kil, H., Paxton, L.J., Pi, X., Hairston, M.R., Zhang, Y., 2003. Case study of the 15 July 2000 magnetic storm effects on the ionosphere-driver of the positive ionospheric storm in the winter hemisphere. J. Geophys. Res. 108 (A11).

Klimenko, M.V., Klimenko, V.V., Ratovsky, K.G., Goncharenko, L.P., 2011. Disturbances in the ionospheric F-region peak heights in the American longitudinal sector during geomagnetic storms of September 2005. Adv. Space Res. 48, 1184–1195.

Li, G., Ning, B., Zhao, B., Liu, L., Liu, J.Y., Yumoto, K., 2008. Effects of geomagnetic storm on GPS ionospheric scintillations at Sanya. J. Atmos. Sol. Terr. Phys. 70, 1034–1045.

Liu, L., Zhao, B., Wan, W., Venkartraman, S., Zhang, M.-L., Yue, X., 2007. Yearly variations of global plasma densities in the topside ionosphere at middle and low latitudes. J. Geophys. Res. 112, A07303. http://dx.doi.org/10.1029/2007JA012283.

Lu, G., Goncharenko, L.P., Richmond, A.D., Roble, R.G., Aponte, N., 2008. A dayside ionospheric positive storm phase driven by neutral winds. J. Geophys. Res. 113, A08304.

Mansilla, G.A., Zossi, M.M., 2013. Ionospheric response to the 3 August 2010 geomagnetic storm at mid and mid-high latitudes. Adv. Space Res. 51, 50–60.

Martinis, C.R., Mendillo, M.J., Aarons, J., 2005. Toward a synthesis of equatorial spread F onset and suppression during geomagnetic storms. J. Geophys. Res. 110, A07306.

Maruyama, N., Richmond, A.D., Fuller-Rowell, T.J., Codrescu, M.V., Sazykin, S., Toffoletto, F.R., Spiro, R.W., Millward, G.H., 2005. Interaction between direct penetration and disturbance dynamo electric fields in the storm-time equatorial ionosphere. J. Geophys. Res. 32, L17105. http://dx.doi.org/10.1029/2005GL023763.

Mendillo, M., Narvaez, C., 2010. Ionospheric storms at geophysically-equivalent sites – Part 2: local time storm patterns for sub-auroral ionospheres. Ann. Geophys. 28, 1449–1462.

Mendillo, M., Lin, B., Aarons, J., 2000. The application of GPS observations to equatorial aeronomy. Radio Sci. 35 (3), 885–904.

Mendillo, M., Rishbeth, H., Roble, R.G., Wroten, J., 2002. Modeling F2-layer seasonal trends and day to day variability driven by coupling with lower atmosphere. J. Atmos. Terr. Phys. v. 64, 1911–1931.

Namgaladze, A.A., Forster, M., Yurik, R.Y., 2000. Analysis of the positive ionospheric response to a moderate geomagnetic storm using a global numerical model. Ann. Geophys. 18, 461–477.

Pi, X., Mannucci, A.J., Lindqwister, U.J., Ho, C.M., 1997. Monitoring of global ionospheric irregularities using the worldwide GPS network. Geophys. Res. Lett. 24, 2283–2286.

Pimenta, A.A., Kelley, M.C., Sahai, Y., Bittencourt, J.A., Fagundes, P.R., 2008. Thermospheric dark band structures observed in all-sky OI 630 nm emission images over the Brazilian low latitude sector. J. Geophys. Res. 113, A01307.

Prölss, G.W., 1993. On explaining the local time variation of ionospheric storm effects. Ann. Geophys. 11, 1–9.

Rajaram, G., Rastoji, R.G., 1970. North-South asymmetry of ionospheric storms-dependence on longitude and season. J. Atmos. Terr. Phys. V 32, 113–118.

Richmond, A.D., Peymirat, C., Roble, R.G., 2003. Long-lasting disturbances in the equatorial ionospheric electric field simulated with a coupled magnetosphere-ionosphere-thermosphere model. J. Geophys. Res. 108 (A3), SIA5/1-SIA5/12.

Sahai, Y., Becker-Guedes, F., Fagundes, P.R., Lima, W.L.C., de Abreu, A.J., Guarnieri, F.L., Candido, C.M.N., Pillat, V.G., 2007b. Unusual ionospheric effects observed during the intense 28 October 2003 solar flare in the Brazilian sector. Ann. Geophys. 25, 2497–2502.

Sahai, Y., Fagundes, P.R., de Jesus, R., de Abreu, A.J., Crowley, G., Kikuchi, T., Huang, C.-S., Pillat, V.G., Guarnieri, F.L., Abalde, J.R., Bittencourt, J., 2011. Studies of

ionospheric F-region response in the Latin American sector during the geomagnetic storm of 21-22 January 2005. Ann. Geophys. 29, 1–11. http://dx.doi.org/10.5194/angeo-29-1-2011.
Sahai, Y., de Jesus, R., Fagundes, P.R., Selhorst, C.L., de Abreu, A.J., Tulasi Ram, S., Aragon-Angel, A., Pillat, V.G., Abalde, J.R., Lima, W.L.C., Bittencourt, J.A., 2012. Effects observed in the equatorial and low latitude ionospheric F-region in the Brazilian sector during low solar activity geomagnetic storms and comparison with the COSMIC measurements. Adv. Space Res. v. 50, 1344–1351.
Sahai, Y., Becher-Guedes, F., Fagundes, P.R., Lima, W.L.C., Otsuka, Y., Huang, C.-S., Espinoza, E.S., Pi, X., de Abreu, A.J., Bolzan, M.J.A., Pillat, V.G., Abalde, J.R., Pimenta, A.A., Bittencourt, J.A., 2007a. Response of nighttime equatorial and low latitude F-region to the geomagnetic storm of August 18, 2003, in the Brazilian sector. Adv. Space Res. v. 39, 1325–1334.
Sastri, J.H., Yumoto, K., Rao, J.V.S., Ikeda, A., 2008. Summer-winter hemisphere asymmetry of the preliminary reverse impulse of geomagnetic storm sudden commencements at midlatitudes. J. Geophys. Res. 113, A05302.
Shagimuratov, I.I., Krankowski, A., Ephishov, I., Cherniak, Yu, Wielgosz, P., Zakharenkova, I., 2012. High latitude TEC fluctuations and irregularity oval during geomagnetic storms. Earth, Planets Space v. 64 (6), 521–529.
Sultan, P.J., 1996. Linear theory and modeling of the Rayleigh–Taylor instability leading to the occurrence of equatorial spread-F. J. Geophys. Res. 101 (A12), 26875–26891.
Takahashi, H., Abdu, M.A., Taylor, M.J., Pautet, P.D., de Paula, E., Kherani, E.A., Medeiros, A.F., Wrasse, C.M., Batista, I.S., Sobral, J.H.A., Gobbi, D., Arruda, D., Paulino, I., Vadas, S., Fritts, D., 2010. Equatorial ionosphere bottom-type spread-F observed by OI 630.0 nm airglow imaging. Geophys. Res. Lett. 37, L03102.
Thomas, E.G., Baker, J.B.H., Ruohoniemi, J.M., Coster, A.J., Zhang, S.-R., 2016. The geomagnetic storm time response of GPS total electron content in the North American sector. J. Geophys. Res. Space Phys. 121, 1744–1759.
Vlasov, M., Kelley, M.C., Kil, H., 2003. Analysis of ground-based and satellite observations of F-region behavior during the great magnetic storm of July, 2000. J. Atmos. Sol. Terr. Phys. 65, 1223–1234.
Wanninger, L., 1993. Effects of the equatorial ionosphere on GPS. GPS World, 48–54.
Whalen, J.A., 2002. Dependence of equatorial bubbles and bottomside spread F on season, magnetic activity, and E×B drift velocity during solar maximum. J. Geophys. Res. 107 (A2), SIA3-1-SIA3-9.
Wu, C.-C., Liou, K., Lepping, R.P., Meng, C.-I., 2004. Identification of substorms within storms. J. Atmos. Sol. Terr. Phys. 66, 125–132.
Yigit, E., Frey, H.U., Moldwin, M.B., Immel, T.J., Ridley, A.J., 2015. Hemispheric differences in the response of the upper atmosphere to the August 2011 geomagnetic storm: a simulation study. J. Atmos. Sol. Terr. Phys. 141, 13–26.
Youssef, M., 2012. On the relation between the CMEs and the solar flares. J. Astron.. Geophys. 1, 172–178.
Yuan, Z.-G., Deng, X.-H., Wang, J.-F., 2008. DMSP/GPS observations of intense ion upflow in the midnight polar ionosphere associated with the SED plume during a super geomagnetic storm. Geophys. Res. Lett. v. 35, L19110.
Zhang, S.-R., et al., 2015. Thermospheric poleward wind surge at midlatitudes during great storm intervals. Geophys. Res. Lett. 42, 5132–5140.